The Role of Metal Substitution in Tuning Anion Redox in Sodium Metal Layered Oxides Revealed by X-Ray Spectroscopy and Theory

Iwnetim Abate[+], Se Young Kim[+], C. Das Pemmaraju, Michael F. Toney, Wanli Yang, Thomas P. Devereaux, William C. Chueh, and Linda F. Nazar**

Abstract: *We investigate high-valent oxygen redox in the positive Na-ion electrode P2-$Na_{0.67-x}[Fe_{0.5}Mn_{0.5}]O_2$ (NMF) where Fe is partially substituted with Cu (P2-$Na_{0.67-x}[Mn_{0.66}Fe_{0.20}Cu_{0.14}]O_2$, NMFC) or Ni (P2-$Na_{0.67-x}[Mn_{0.65}Fe_{0.20}Ni_{0.15}]O_2$, NMFN). From combined analysis of resonant inelastic X-ray scattering and X-ray near-edge structure with electrochemical voltage hysteresis and X-ray pair distribution function profiles, we correlate structural disorder with high-valent oxygen redox and its improvement by Ni or Cu substitution. Density of states calculations elaborate considerable anionic redox in NMF and NMFC without the widely accepted requirement of an A-O-A′ local configuration in the pristine materials (where A = Na and A′ = Li, Mg, vacancy, etc.). We also show that the Jahn–Teller nature of Fe^{4+} and the stabilization mechanism of anionic redox could determine the extent of structural disorder in the materials. These findings shed light on the design principles in TM and anion redox for positive electrodes to improve the performance of Na-ion batteries.*

Introduction

Li-ion batteries (LIBs) are promising devices for both the transportation and utility sectors as they provide high energy density capability to store intermittent renewable sources of energy. However, the high abundance of sodium (100 times that of Li)[1] and compatibility of a sodium anode with an aluminum current collector—which is lower cost than copper collectors used in LIBs—makes Na ion batteries (NIBs) viable options for large-scale applications.

Recently, low-cost and non-toxic NIBs made from Mn and Fe have drawn considerable attention in the battery community.[2] Yabuuchi et al. demonstrated the effectiveness of layered oxide P2-$Na_{2/3}[Fe_{0.5}Mn_{0.5}]O_2$ as a positive electrode material. It delivers a reversible capacity of 190 $mAh\,g^{-1}$ at room temperature with charge compensation that was presumed to be through $Fe^{3+/4+}$ redox.[2a] The considerably improved electrochemical reversibility compared with that of Li-ion positive electrodes such as $LiFeO_2$ demonstrated the potential of sodium-based electrodes to deliver high capacity using earth-abundant materials such as Fe and Mn. However, the practical use of these materials is inhibited by their reactivity with moisture and CO_2 in air[2e] as well as their structural instability[2b,3] upon deep desodiation. In the pristine materials, the transition metals (TMs), Fe and Mn, reside in octahedral sites in the TMO_2 layer. However, X-ray and neutron diffraction studies have shown that the TMs shuffle into tetrahedral sites in the Na layers upon desodiation, leading to structural degradation, capacity fade, and decreased rate capability.[2b,c] Although partial substitution of Fe with Mn, Ni, Co, Cu, or Ti has been shown to mitigate these issues,[2b,c,4] a full understanding of the effect of TM substitution on structural stability-redox coupling has remained elusive.

Similar to the case of Li layered TM oxides, improving capacity by accessing both cationic and anionic redox has been demonstrated in several Na-ion layered TM oxides. The often-discussed requirement for anionic redox is the presence of A-O-A′ (where A stands for an alkali metal and A′ stands for species with no covalent bonding interaction with the oxygen; for example, Li-O-Li, Na-O-Mg/Zn or Na-O-Vacancy) local configurations in positive electrode materials.[5] The configuration has been linked to the formation of nonbonding oxygen 2p states below the Fermi-level which will participate in charge compensation upon charging. This proposal has been adopted to explain the anionic redox activity in sodium

[*] S. Y. Kim,[+] Prof. L. F. Nazar
Department of Chemistry and the Waterloo Institute for Nanotechnology, University of Waterloo
Waterloo, Ontario N2L 3G1 (Canada)
E-mail: lfnazar@uwaterloo.ca
I. Abate,[+] Dr. M. F. Toney, Prof. T. P. Devereaux, Prof. W. C. Chueh
Department of Materials Science and Engineering, Stanford University
496 Lomita Mall, Stanford, CA 94305 (USA)
E-mail: wchueh@stanford.edu
I. Abate,[+] Dr. C. D. Pemmaraju, Prof. T. P. Devereaux, Prof. W. C. Chueh
Stanford Institute for Materials & Energy Sciences, SLAC National Accelerator Laboratory
2575 Sand Hill Road, Menlo Park, CA 94025 (USA)
Dr. M. F. Toney
Stanford Synchrotron Radiation Light Source, SLAC National Accelerator Laboratory
2575 Sand Hill Road, Menlo Park, CA 94025 (USA)
Dr. W. Yang
Advanced Light Source, Lawrence Berkeley National Laboratory
Berkeley, CA 94720 (USA)
[+] These authors contributed equally to this work.

Supporting information and the ORCID identification number(s) for the author(s) of this article can be found under: https://doi.org/10.1002/anie.202012205.

electrode materials such as $Na_{0.6}Li_{0.2}Mn_{0.8}O_2$, Na_2RuO_3, $Na_2Mn_3O_7$ $Na_{0.67}Mg_{0.28}Mn_{0.72}O_2$. $Na_{0.67}Zn_{0.28}Mn_{0.72}O_2$ and $Na_{0.78}Ni_{0.23}Mn_{0.69}O_2$.[5] However, anionic redox has also been linked with structural disorder[6] that results in voltage hysteresis and fade of both voltage and capacity, impeding its practicality in devices.[6,7] Recently, House et al. showed that superstructure control in sodium positive electrodes could mitigate the structural disorder linked with anionic redox.[8] Another report by Song et al. examined the oxygen density of states (DOS) of ordered Li_2TMO_3 (TM = 3d TMs) compounds and proposed that TMs surrounding a Li-O-Li local configuration have a nontrivial π-type interaction with oxygen which modulates the energy level of O 2p and TM t_{2g} states. Based on the DOS results, they further demonstrated that oxygen redox activity could be estimated by the types and numbers of the TMs surrounding Li-O-Li in Li_2TMO_3 systems.[9] Although partial metal substitution has been generally used to diminish structural disorder on cycling,[2b,c,4] a design rule that involves a specific metal or synthesis method is further needed to be developed to disrupt the link of structure-redox coupling in anionic redox positive electrode materials.

Previously, some of us examined the effect of substituting Fe by Cu and Ni in P2-$Na_{0.67-x}[Mn_{0.5}Fe_{0.5}]O_2$ (NMF) on electrochemical performance,[2b,c] showing that Ni was particularly effective in controlling capacity fade. In P2-$Na_{0.67-x}[Mn_{0.66}Fe_{0.20}Cu_{0.14}]O_2$ (NMFC) and P2-$Na_{0.67-x}[Mn_{0.65}Fe_{0.20}Ni_{0.15}]O_2$ (NMFN), charge compensation on charge would be typically achieved by transition metal redox. However, our studies hinted that oxygen redox also occurs in NMF and NMFC, accompanied by the TMs migrating from octahedral sites (pristine state) to tetrahedral sites (desodiated state).[2b,c] Such site swapping (i.e., TM migration) is only partly reversible.

As part of a "deep dive" into understanding redox mechanisms in positive electrodes on electrochemical cycling, here we prove the existence of anion-redox activity in NMF, and its modification by Cu/Ni substitution. By combining analysis of local structure with spectroscopic probes—specifically, resonant inelastic X-ray scattering (RIXS) and X-ray near edge structure (XANES)—we show how TM substitution tunes the structure-redox relationship. We unveil the structure-redox link in NIBs, further corroborating this relationship that has been previously observed in LIBs in electrode materials such as $Li_{1.17-x}Ni_{0.21}Co_{0.08}Mn_{0.54}O_2$[6] and $Li_xIr_ySn_{1-y}O_2$.[10] We find that substitution is a vital strategy to lower structural disorder in the presence of anionic redox, by reducing Jahn–Teller distortion due to Fe^{+4} and modulating the TM-O covalency. In addition, by performing density-functional theory (DFT) calculations, we explore why NMF and NMFC exhibit considerable anionic redox even though they do not satisfy the widely accepted requirement of a local A-O-A′ configuration (Li-O-Li, Na-O-Mg/Zn or Na-O-Vacancy) in the pristine materials.[5e,11]

Results and Discussion

To provide background, the electrochemical properties and X-ray pair distribution function (PDF) analysis of the NMF, NMFC and NMFN electrodes are compared in Figure 1. P2-type layered $Na_{0.67}TMO_2$ encounters a change in stacking order during desodiation. A phase transition from the P2 to a very poorly crystalline O2-like phase (hereafter, called the Z-phase) occurs on deep charge as we previously reported (Figure S1).[2b,c] The changes in the first cycle are

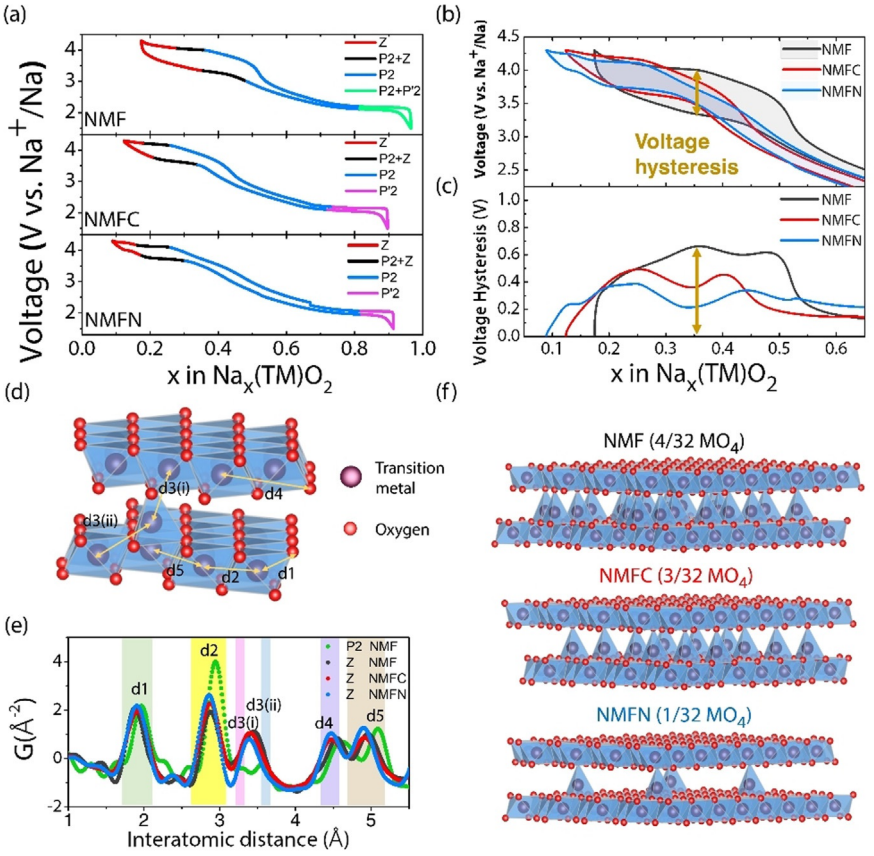

Figure 1. Effect of TM substitution on electrochemistry. a) First cycle electrochemistry for NMF, NMFC, and NMFN cycled at 0.1 C. b and c) Comparison of the first cycle and voltage hysteresis upon desodiation, respectively, of the three electrodes cycled at 0.1 C. The substitution of Fe with Cu or Ni in $Na_{0.67}Mn_{0.5}Fe_{0.5}O_2$ reduces the hysteresis gap and pushes the start of the plateau at high voltage to higher voltage. d) Scheme of the bilayer model used to fit the pair distribution function (PDF) curve of NMF, NMFC, and NMFN. The purple and red spheres represent the transition metals and oxygen atoms, respectively. The yellow arrows indicate the atomic distance, as labeled. e) Comparison of the experimental X-ray PDF data of pristine P2-NMF with Z-phase NMF, NMFC, and NMFN. f) Schematic models of Z-phase NMF, NMFC, and NMFN. The antisite-vacancy defect (AVDF) formation in NMF is mitigated by substituting Fe with Cu or Ni.

summarized and depicted in different colors in Figure 1a. Here, to rigorously assess voltage hysteresis between sodiation and desodiation, we performed cycling at different rates (1 C, 0.5 C, 0.1 C and 0.05 C; Figure S2). While hysteresis is more dominant at the faster C-rates as expected, it is still quite significant for NMF at and below 0.1 C (i.e. at 0.05 C). This indicates a kinetic limitation due to TM shuffling into the tetrahedral sites (as previously described for lithium metal oxides)[12] and formation of so-called antisite-vacancy defects (AVDF)[6] discussed below. Above 3.1 V, the hysteresis gap amongst the three electrodes diverge, shown in Figure 1b. To directly compare the voltage hysteresis, the voltage difference at a given state-of-charge was quantified (Figure 1c). The largest hysteresis occurs during the P2 to Z phase transformation at a Na composition of $\approx$0.35, $\approx$0.25 and $\approx$0.25 mol for NMF, NMFC and NMFN, respectively. Substitution of Ni decreases the maximum hysteresis from 0.66 V to 0.38 V. Thus the hysteresis is the greatest in NMF, followed by NMFC and then NMFN.

To elucidate the underlying factors governing the difference in voltage hysteresis, first, we re-visited the local structure of the Z-phase in the three P2-oxides. X-ray PDF analysis quantifies the amount of AVDF in chemically desodiated samples, i.e., the degree of TM migration.[2c] For simplicity, we assumed the total mass of the AVDF pair is preserved in the structure during the Z-phase evolution. The PDF curve fitting (Figure S3) was conducted by adopting a $4 \times 4 \times 10$ supercell extended from an O2-type bilayer model in Figure 1d, whose origin was described previously.[2b,c] The decreased intensity of the d3(i) and d3(ii) PDF peaks in Figure 1e in NMFC and NMFN compared with that of NMF confirms that the AVDF concentration in the Z-phase decreases upon Cu or Ni substitution.[2c] The corresponding bilayer models of the Z-phases from each material are displayed in Figure 1f. The effect of Cu or Ni substitution—namely to reduce AVDF formation in the NMFC and NMFN electrodes—is reflected in a lower voltage hysteresis evolution upon forming the Z-phase. This suggests that the two factors are linked.

Redox Mechanism: Role of Anionic Redox in Charge Compensation

To understand why Cu and Ni substitution affect the voltage hysteresis and the concentration of the AVDFs, insight into the redox behavior of each element is needed. XANES and RIXS have been widely used to investigate element-specific redox behavior and to correlate structural evolution and oxidation state change in TM oxide materials. In our previous reports,[2b,c] the possible involvement of lattice oxygen in the redox behavior of NMF and NMFC was inferred from in situ XANES measurements at the Mn, Fe and Cu K-edges along with ^{57}Fe Mössbauer spectroscopy analysis. In these studies, the XANES spectra of each cation showed a shift to higher energy upon charge to 4.1 V, but further desodiation to 4.3 V did not result in any discernible energy shift in the spectra.[2a,c] Here, we employ TM XANES studies to probe the behavior of the Ni-analogue, NMFN (Figure S4). The Ni K-edge XANES spectra in Figure S4(a) demonstrate that Ni is oxidized, compensating for charge at potentials above 4.1 V. This is evidenced by a white line shift from 8352 eV to 8355 eV ($Ni^{2+/4+}$) and decreasing peak maxima which are typical redox features of Ni, in agreement with previous observations of P2-$Na_{2/3}[Ni_{1/3-y/2}Mn_{2/3-y/2}Fe_y]O_2$ and O3-$NaFe_{0.3}Ni_{0.7}O_2$.[13] These results confirm that the high-voltage, Z-phase capacity in NMFN involves significant TM (specifically Ni) redox, whereas this is not the case for NMF and NMFC.[2b,c] It suggests that the NMFN Z-phase is inactive for anion redox, while NMF and NMFC are active.

To directly quantify the extent of oxygen redox, RIXS at the O K edge was conducted on each electrode at different states during the first oxidation cycle. Points were chosen between 3.9 and 4.3 V (Figure 1a) to sample the uppermost state of charge. RIXS has been used extensively to determine the presence of depopulated O 2p states in Li and Na oxides.[6,10,11e,14] By combining XANES and RIXS analyses on the TMs and oxygen, respectively, we can explore the correlation between cation disorder and cation/anion redox.

RIXS maps for NMF charged to between 3.9 and 4.3 V are shown in Figure 2. In pristine NMF, we observed two excitations involving intermediate state transitions into the unoccupied hybridized TM 3d-O 2p* and TM 4sp-O 2p* states appearing at approximately 528–533 eV and $>$535 eV in excitation energy, respectively. Accompanying emission occurs at approximately 522–527 eV due to decay from the relatively broad (delocalized) oxygen valence band states to fill the excited O 1s core hole.[14] The TM 3d-O 2p* features corresponds to the pre-edge of O-K edge spectroscopy and is dominated by TM 3d character through a strong TM-O hybridization effect which evolves during cationic redox (Figure S7).[14,15]

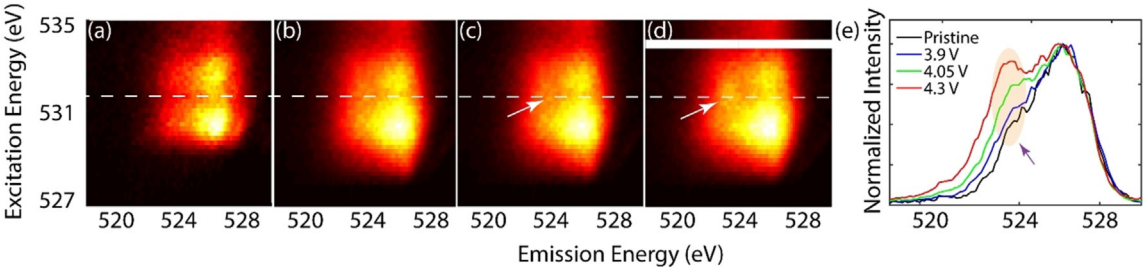

Figure 2. O K-edge RIXS measurement of NMF. a–d) RIXS maps of the pristine electrode and of electrodes at 3.9, 4.05, and 4.3 V, respectively. A white dotted line is drawn across the maps to indicate the region of the map ($\approx$531.5 eV in excitation energy) where the anionic redox feature should be located. e) Integration of the map at $\approx$531.5 eV excitation. The integration reveals a localized shoulder at approximately 523 eV in emission energy. Therefore, oxygen is involved in compensation of charge during desodiation above 3.9 V.

The O K-edge RIXS map of NMF at 3.9 V (Figure 2b) reveals similar excitation and emission states to the pristine electrode. In contrast, for electrodes desodiated to 4.05 and 4.3 V, a sharp feature appears at 531.5 eV in excitation and at 523.3 eV in emission, which differs from the broad 522–527 eV emission features. This localized feature has been linked to anionic redox.[2a,h,6,10,11e,16] To further examine this feature, single-energy RIXS spectra at an excitation energy of 531.5 eV were obtained (Figure 2e). A peak emerges at an emission energy of ≈523 eV and grows with voltage, indicating anionic oxidation above 3.9 V. The oxygen redox suggested here is consistent with the absence of Mn and Fe redox activity in XANES in the same voltage range.[2a,c]

Similar to NMF, the RIXS evolution in NMFC confirms the existence of an oxygen redox feature in the 4.3 V-charged electrode (Figure 3d). However, the oxygen redox feature from the single-energy RIXS spectra at 531.5 eV excitation energy in Figure 3e indicates that the onset of oxygen oxidation occurs at a higher voltage than in NMF, specifically, above ≈4.15 V.

In contrast to NMF and NMFC, the O-K edge RIXS maps of NMFN exhibit no discernible oxygen redox feature upon desodiation to 4.3 V, which is also confirmed by the single-energy RIXS spectra (Figure 4). Consistent with this finding is that the Ni K-edge XANES white line shifts by 3 eV between 4 and 4.3 V (Figure S4). This confirms that Ni oxidation, rather than that of oxygen, occurs upon desodiation of NMFN at high voltage (>4.1 V).

We summarize the redox mechanism in the three electrodes by combining the XANES, RIXS and Mössbauer spectroscopy (Fe) results from this and previous studies in Figure 5a.[2a–c] We followed two methods to quantify oxygen's involvement in redox. First, we calculated how much capacity is unaccounted for by the TM redox from XANES and Mössbauer spectroscopy. The extent of oxygen redox is here defined as the number of electrons per oxygen that contribute to charge compensation during desodiation (Figure 5b). Second, we analyzed the intensity of the anionic redox feature in the single energy RIXS spectra. Both methods resulted in the same trend for the extent of anionic redox: NMFC ≥ NMF ≫ NMFN. Variations of capacity from cell to cell and limits of instrument resolution were used to estimate error bars. Details of these analyses, including quantification procedures, are explained in Table S1 and Figure S6.

Structure-Anionic Redox Link

Our combined structural and spectroscopic characterizations suggest a significant fraction of antisite-vacancy defects form on initial desodiation in NMF and NMFC, and are accompanied by anionic oxidation. On the other hand, NMFN exhibits Ni oxidation and does not form such discernible defects. This observation from the sodium layered oxide positive electrodes mirrors the structure-anionic redox link reported for Li layered oxide positive electrodes.[6,10,,11e,14a,17] The correlation suggests that AVDF formation could be one form of local structure stabilization during oxygen activity.[10,18] Before we discuss what determines the extent of defect formation in these materials, we first address why we observed anionic redox in NMF/C, contrary to prediction based on previous models.

A local configuration of A-O-A′ (Li-O-Li, Na-O-Mg/Zn or Na-O-Vacancy) in the reduced materials has been pro-

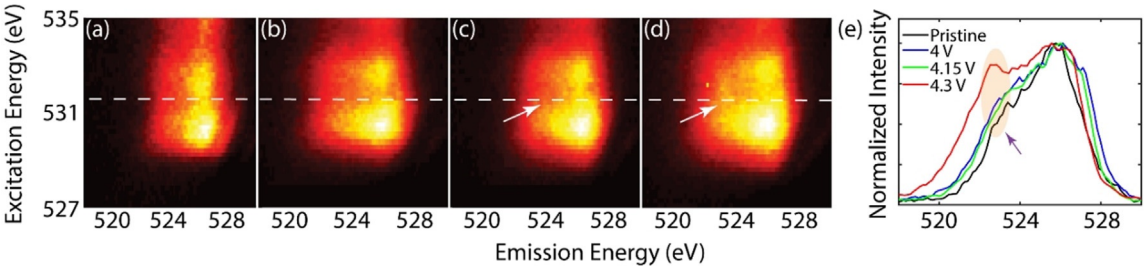

Figure 3. O K-edge RIXS measurement of NMFC. a–d) RIXS maps of the pristine electrode and of electrodes at 4, 4.15, and 4.3 V, respectively. e) Integration of the map at 531.5 eV (white line in (b)–(e)). The integration reveals a localized shoulder appearing at approximately 523 eV in emission energy, indicating that oxygen is involved in charge compensation during desodiation above 4.15 V.

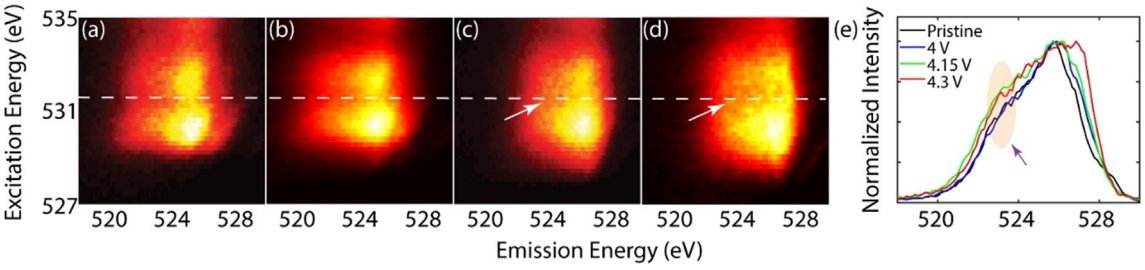

Figure 4. O K-edge RIXS measurement of NMFN. a–d) RIXS maps of the pristine electrode and of electrodes at 4, 4.15, and 4.3 V, respectively. e) Integration of the map at 531.5 eV (white line in (a)–(d)). The integration reveals no localized shoulder appears at approximately 523 eV in emission energy. Therefore, oxygen involvement in charge compensation during desodiation at higher voltage is negligible.

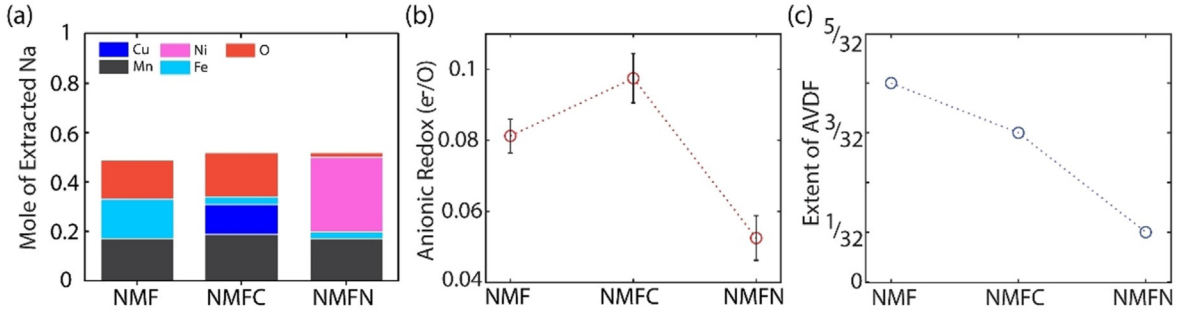

Figure 5. a) Summary of charge compensation in the three electrodes. b) The extent of anion redox (e^-/O). c) The extent of AVDF formation (fraction of TMs that swap their position from the octahedral sites in the TM layer to tetrahedral sites in the Na layer.).

posed as a requirement for anionic redox. This configuration can form a narrow non-bonding O 2p state that can participate in anionic redox.[5e,11] In this requirement, A and A′ have to be redox inactive metals and the A–O bond has to be relatively ionic, so that electrons that form the bond are highly polarized (and more localized on the oxygen anions). Based on this supposition, NMF, NMFC and NMFN are not expected to exhibit anionic redox due to the absence of this specific configuration. However, our experimental results suggest otherwise. Thus, we performed density of states (DOS) calculations to shed light on the factors that control the fraction of oxygen activity during charging. We reduced the number of transition metals in each composition to simplify the calculation and explore the role of a given metal. We kept the Mn content to be $^1/_2$ of the transition metal sites and filled the other $^1/_2$ with Fe, Ni, or Cu. This systematic exploration allows us to clearly correlate the changes in the DOS with the type of transition metal. Using three metals per material would make it harder to isolate the role of each. Figure 6 shows the DOS of $Na_{2/3}Mn_{1/2}Fe_{1/2}O_2$ (NMF), $Na_{2/3}Mn_{1/2}Cu_{1/2}O_2$ (NMC), and $Na_{2/3}Mn_{1/2}Ni_{1/2}O_2$ (NMN). The integrated partial DOS between −1.5 eV and 0 eV was analyzed to estimate how much a given band dominates near the Fermi level (giving an estimate of the fraction of electrons available for redox) (Figure 6d). The extent to which the oxygen band dominates the band near the Fermi level is in the following order: $O_{NMC} > O_{NMF} > O_{NMN}$. We note that these calculations are for the pristine materials prior to desodiation. As the charged state is highly disordered and not structurally resolvable, we could not perform DFT. Nonetheless, based on the DOS, we expect Cu and Fe containing materials to have more oxygen-electron availability for redox than Ni during desodiation of the corresponding positive electrode. This is consistent with our experimental observation where the extent of anionic redox follows the order NMFC ≥ NMF ≫ NMFN. This finding corroborates the reliability of our theoretical analysis to predict the redox behavior upon cycling based on the structure of the pristine material.

The relative contribution of a given band near a Fermi level can also be understood as the relative location of the band's centroid (Figure 6e). The more the band dominates, the closer is its centroid to the Fermi level. The effect of the location of the centroid of the band (with respect to the Fermi level) on the surface exchange kinetics – in fuel cells, electrolysis cells[19] and on catalysis activity for the oxygen evolution reaction[20] – has also been previously reported. While the A-O-A′ configuration forms a nonbonding oxygen 2p state close to the Fermi level and thereby increases the extent of oxygen participation in redox, our work here shows that chemical substitution is an effective knob to tune oxygen participation. The type of transition metal, the strength of covalency and local symmetry (among other factors) can play a role in enhancing the presence of O 2p states near the Fermi level. For example, NMF, NMFC and NMFN—despite similar local structure and stoichiometry—have different oxygen band dominance near the Fermi level due to the difference in the transition metal. This introduces oxygen dominance near

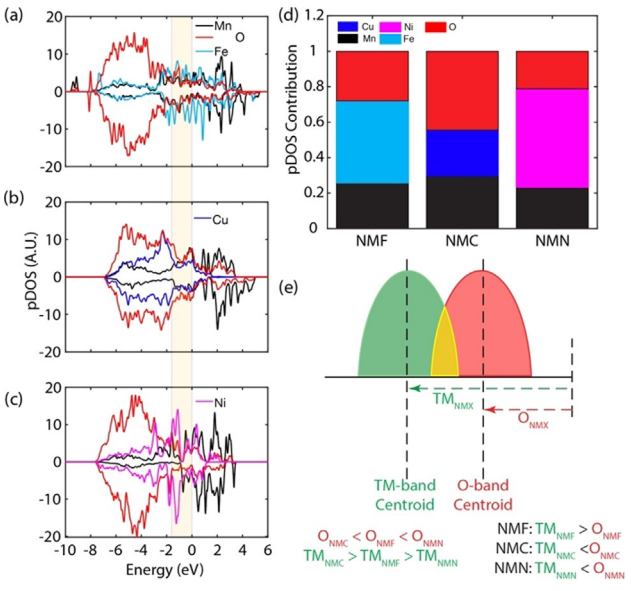

Figure 6. DOS calculation for NMF, NMC, and NMN (a), (b) and (c). The area under a given band was calculated between −1.5 eV and 0 eV (highlighted region) to estimate the DOS contribution of each elements (d). From the electrochemistry, we expect to extract ≈0.5 electrons during this voltage window, and we estimated the −1.5 eV to 0 eV range in the pDOS will contribute to this number of electrons. The DOS contribution of both TM and O is consistent with the respective charge compensation obtained from experiment (Figure 5a). (e) Schematic summarizing the O-band dependence of the extent of anionic redox. The more oxygen 2p states near the Fermi level, the more their relative contribution to charge compensation (extent of anionic redox). The respective O 2p and TM 3d state contribution compared in the schematic diagram is based on the integrated values from the pDOS between −1.5 to 0 eV.

the Fermi level as a more general descriptor to determine the extent of anionic redox. We recognize that structural changes upon desodiation may affect the electronic structure and thereby slightly alter the relative cationic and anionic charge compensation mechanism in the resulting oxidized species.[21] However, while our calculations are conducted on the pristine material, the relative partial DOS contribution near the Fermi level (Figure 6d) and the charge compensation by the respective ions determined from experiment (Figure 5a) are strikingly similar, confirming the robustness of this method.

The degree of AVDF and the extent of anionic redox are not correlated in a 1:1 manner. The trend in the degree of AVDF is NMF > NMFC > NMFN, whereas the trend in the extent of anionic redox is NMFC ≥ NMF ⩾ NMFN. This suggests that there is an additional factor that plays a role in determining the extent of AVDF.

Despite its lower anionic activity, the extent of AVDF in NMF is higher than NMFC. We propose the higher concentration of Jahn–Teller active Fe^{4+} ions per formula unit in NMF than NMFC can explain this for two main reasons:

1. Jahn–Teller active Fe^{4+} facilitates the AVDF formation by lowering the energy barrier for TMs to migrate from the octahedral sites in the TMO_2 layer to tetrahedral sites in the Na layer as illustrated in Figure 7a.[22] Poor cycling of O3-$NaFeO_2$ has also been ascribed to Jahn–Teller induced AVDF.[23] The presence of a non-cooperative Jahn–Teller effect of high-spin Fe^{4+} in NMF was previously reported[2a] based on the Debye-Waller factor extracted from EXAFS. We have also confirmed local structural changes in NMFC/N using EXAFS (Figure S5).
2. Stabilizing the Fe^{4+} ion by ligand metal charge transfer promotes weakening of the TM–O bonding to neighboring TM atoms.[24] Thus, it increases susceptibility to AVDF formation by TM migration in NMF as shown in Figure 7b.

Comparing NMFC and NMFN, anionic redox is more significant in the former than the latter which means the structural changes that could take place to stabilize the oxidized species (such as oxygen dimer or TM = O formation[10,17a,18]) are more significant in NMFC. The combination of these two phenomena describes the AVDF trend observed, NMF > NMFC > NMFN (Figure 5c), although the trend for the extent of anionic redox is NMFC ≥ NMF ⩾ NMFN (Figure 5b).

Conclusion

Our investigation of the effect of transition metal substitution in sodium layered metal oxides based on P2-$Na_{0.67-x}[Mn_{0.5}Fe_{0.5}]O_2$ (NMF) reveals the complex interplay of the factors that control electrochemical behavior in this material. The study disentangles the complex contributions of anion redox and TM migration to establish a relationship between structural disorder and oxygen redox. It demonstrates why partial substitution is a viable method to design Fe based compounds with optimal composition and good properties—a design that takes into account the role of anion redox.

First, the combination of experiment (RIXS, XANES, electrochemistry and PDF analysis) together with theory (density-of-state calculations) indisputably prove the contribution of anion redox and evaluate its effect. While iron-rich sodium metal oxides are a cost-effective, environmentally beneficial choice as Na-battery cathodes, they suffer structural hysteresis on deep charge. This owes to formation of significant antisite-vacancy defects (AVDF) and oxygen anion redox activity in the high-valent state, which results in structural disorder that is further triggered by the Jahn–Teller nature of Fe^{+4}.

While an A-O-A′ local structure can increase the amount of O 2p states near the Fermi level, it is not a necessary condition for oxygen redox in the P2 sodium layered TM oxides as previously thought. NMF and its Cu-substituted analogue lack this configuration yet have significant anionic redox. DOS calculations show that anion redox is more favored if the oxygen 2p band dominates the band near the Fermi level in the TM–O bond. The more oxygen 2p states near the Fermi level, the more their relative contribution to charge compensation. Consequently, the covalency of the TM, among other factors, can increase the oxygen density near the Fermi level and thereby the propensity for anionic redox.

Reducing the concentration of Fe^{+4} ions in the charged state via their partial substitution is necessary to alter

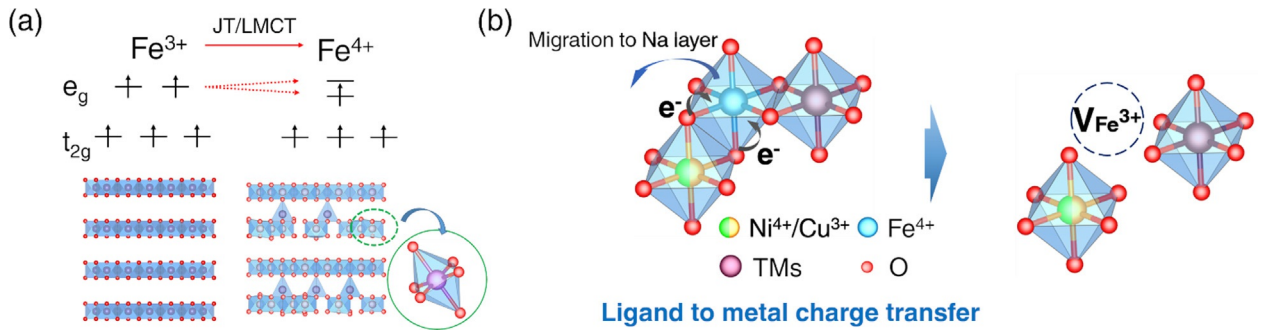

Figure 7. Schematic showing the correlation between out-of-plane disorder and concentration of Fe^{4+} ions. a) JT-assisted distortion could reduce the energy barrier for disorder by reducing the energy difference between the octahedral sites in the TM layer and prismatic sites in the sodium layer.[18] b) Schematic of the Fe^{3+} migration process by LMCT of Cu/Ni in NMFC or NMFN. LMCT weakens the metal-oxygen bond, which enables the disordering of TMs out of the TMO_2 layers.

composition, and hence tune anion redox and affect structural stability-redox coupling. We outlined two approaches here: 1) choosing a TM substituent which minimizes AVDF but optimizes anion redox (e.g. Cu); 2) choosing a TM substituent whose band is closer to the Fermi level than the oxygen band in order to suppress anion redox and AVDF formation (e.g. Ni). While it isn't yet clear which strategy is best, we believe our understanding of the mechanisms at play sheds light on design principles and can guide future directions to improve the performance of sodium-ion battery positive electrodes.

Acknowledgements

L.F.N. would like to thank the Natural Sciences and Engineering Council of Canada for generous financial support of this work through their Discovery and Canada Research Chair programs. W.C.C., T.P.D, I.I.A. and C.D.p. would like to acknowledge the U.S. Department of Energy (DOE), Office of Basic Energy Sciences, Division of Materials Sciences and Engineering (contract DE-AC02-76SF00515) for their support. I.I.A. was additionally supported by the Stanford DARE fellowship program. Use of the ALS was supported by the Office of Science, Office of Basic Energy Sciences, of the US DOE under contract no. DE-AC02-05CH11231. Use of the SSRL, SLAC National Accelerator Laboratory, was supported by the Office of Science, Office of Basic Energy Sciences, of the US DOE under contract no. DE-AC02-76SF00515. Part of this work was performed at the Stanford Nano Shared Facilities, supported by the National Science Foundation under award ECCS-1542152. The computational work used resources at the National Energy Research Scientific Computing Center (NERSC), a U.S. DOE Office of Science User Facility operated under contract no. DE-AC02-05CH11231.

Conflict of interest

The authors declare no conflict of interest.

Keywords: anion redox · ligand metal charge transfer · nonbonding O 2p state · sodium ion batteries · structure-redox coupling

[1] C. Vaalma, D. Buchholz, M. Weil, S. Passerini, *Nat. Rev. Mater.* **2018**, *3*, 18013.

[2] a) N. Yabuuchi, M. Kajiyama, J. Iwatate, H. Nishikawa, S. Hitomi, R. Okuyama, R. Usui, Y. Yamada, S. Komaba, *Nat. Mater.* **2012**, *11*, 512 – 517; b) E. Talaie, V. Duffort, H. L. Smith, B. Fultz, L. F. Nazar, *Energy Environ. Sci.* **2015**, *8*, 2512 – 2523; c) E. Talaie, S. Y. Kim, N. Chen, L. F. Nazar, *Chem. Mater.* **2017**, *29*, 6684 – 6697; d) D. D. Yuan, X. H. Hu, J. F. Qian, F. Pei, F. Y. Wu, R. J. Mao, X. P. Ai, H. X. Yang, Y. L. Cao, *Electrochim. Acta* **2014**, *116*, 300 – 305; e) V. Duffort, E. Talaie, R. Black, L. F. Nazar, *Chem. Mater.* **2015**, *27*, 2515 – 2524; f) S. Kalluri, K. H. Seng, W. K. Pang, Z. P. Guo, Z. X. Chen, H. K. Liu, S. X. Dou, *ACS Appl. Mater. Interfaces* **2014**, *6*, 8953 – 8958; g) E. Gonzalo, M. H. Han, J. M. L. del Amo, B. Acebedo, M. Casas-Cabanas, T. Rojo, *J. Mater. Chem. A* **2014**, *2*, 18523 – 18530; h) B. Mortemard de Boisse, D. Carlier, M. Guignard, L. Bourgeois, C. Delmas, *Inorg. Chem.* **2014**, *53*, 11197 – 11205; i) B. Mortemard de Boisse, D. Carlier, M. Guignard, C. Delmas, *J. Electrochem. Soc.* **2013**, *160*, A569 – A574; j) J. T. Xu, S. L. Chou, J. L. Wang, H. K. Liu, S. X. Dou, *ChemElectroChem* **2014**, *1*, 371 – 374.

[3] D. Susanto, M. K. Cho, G. Ali, J. Y. Kim, H. J. Chang, H. S. Kim, K. W. Nam, K. Y. Chung, *Chem. Mater.* **2019**, *31*, 3644 – 3651.

[4] a) D. Kim, E. Lee, M. Slater, W. Q. Lu, S. Rood, C. S. Johnson, *Electrochem. Commun.* **2012**, *18*, 66 – 69; b) H. Yoshida, N. Yabuuchi, S. Komaba, *Electrochem. Commun.* **2013**, *34*, 60 – 63; c) S. Y. Xu, X. Y. Wu, Y. M. Li, Y. S. Hu, L. Q. Chen, *Chin. Phys. B* **2014**, *23*, 118202; d) M. H. Han, E. Gonzalo, N. Sharma, J. M. L. del Amo, M. Armand, M. Avdeev, J. J. S. Garitaonandia, T. Rojo, *Chem. Mater.* **2016**, *28*, 106 – 116; e) Y. Ono, Y. Yui, M. Hayashi, K. Asakura, H. Kitabayashi, K. I. Takahashi, *ECS Trans.* **2014**, *58*, 33 – 39; f) D. Kundu, E. Talaie, V. Duffort, L. F. Nazar, *Angew. Chem. Int. Ed.* **2015**, *54*, 3431 – 3448; g) L. Liu, X. Li, S. H. Bo, Y. Wang, H. L. Chen, N. Twu, D. Wu, G. Ceder, *Adv. Energy Mater.* **2015**, *5*, 1500944.

[5] a) K. Du, J. Y. Zhu, G. R. Hu, H. C. Gao, Y. T. Li, J. B. Goodenough, *Energy Environ. Sci.* **2016**, *9*, 2575 – 2577; b) X. H. Rong, J. Liu, E. Y. Hu, Y. J. Liu, Y. Wang, J. P. Wu, X. Q. Yu, K. Page, Y. S. Hu, W. L. Yang, H. Li, X. Q. Yang, L. Q. Chen, X. J. Huang, *Joule* **2018**, *2*, 125 – 140; c) B. M. de Boisse, G. D. Liu, J. T. Ma, S. Nishimura, S. C. Chung, H. Kiuchi, Y. Harada, J. Kikkawa, Y. Kobayashi, M. Okubo, A. Yamada, *Nat. Commun.* **2016**, *7*, 11397; d) W. Zheng, Q. Liu, Z. Y. Wang, Z. B. Yi, Y. Z. Li, L. J. Cao, K. L. Zhang, Z. G. Lu, *J. Power Sources* **2019**, *439*, 227086; e) X. Bai, M. Sathiya, B. Mendoza-Sanchez, A. Iadecola, J. Vergnet, R. Dedryvere, M. Saubanere, A. M. Abakumov, P. Rozier, J. M. Tarascon, *Adv. Energy Mater.* **2018**, *8*, 1802379; f) C. Z. Ma, J. Alvarado, J. Xu, R. J. Clement, M. Kodur, W. Tong, C. P. Grey, Y. S. Meng, *J. Am. Chem. Soc.* **2017**, *139*, 4835 – 4845; g) B. M. de Boisse, M. Reynaud, J. T. Ma, J. Kikkawa, S. I. Nishimura, M. Casas-Cabanas, C. Delmas, M. Okubo, A. Yamada, *Nat. Commun.* **2019**, *10*, 2185.

[6] W. E. Gent, K. Lim, Y. F. Liang, Q. H. Li, T. Barnes, S. J. Ahn, K. H. Stone, M. McIntire, J. Y. Hong, J. H. Song, Y. Y. Li, A. Mehta, S. Ermon, T. Tyliszczak, D. Kilcoyne, D. Vine, J. H. Park, S. K. Doo, M. F. Toney, W. L. Yang, D. Prendergast, W. C. Chueh, *Nat. Commun.* **2017**, *8*, 2091.

[7] G. Assat, S. L. Glazier, C. Delacourt, J. M. Tarascon, *Nat. Energy* **2019**, *4*, 647 – 656.

[8] R. A. House, U. Maitra, M. A. Pérez-Osorio, J. G. Lozano, L. Jin, J. W. Somerville, L. C. Duda, A. Nag, A. Walters, K. J. Zhou, M. R. Roberts, P. G. Bruce, *Nature* **2020**, *577*, 502 – 508.

[9] J. H. Song, G. Yoon, B. Kim, D. Eum, H. Park, D. H. Kim, K. Kang, *Adv. Energy Mater.* **2020**, *0*, 2001207.

[10] J. Hong, W. E. Gent, P. Xiao, K. Lim, D. H. Seo, J. Wu, P. M. Csernica, C. J. Takacs, D. Nordlund, C. J. Sun, K. H. Stone, D. Passarello, W. L. Yang, D. Prendergast, G. Ceder, M. F. Toney, W. C. Chueh, *Nat. Mater.* **2019**, *18*, 256 – 265.

[11] a) D. H. Seo, J. Lee, A. Urban, R. Malik, S. Kang, G. Ceder, *Nat. Chem.* **2016**, *8*, 692 – 697; b) G. Assat, J. M. Tarascon, *Nat. Energy* **2018**, *3*, 373 – 386; c) U. Maitra, R. A. House, J. Somerville, N. Tapia-Ruiz, J. G. Lozano, N. Guerrini, R. Hao, K. Luo, L. Y. Jin, M. A. Perez-Osorio, F. Massel, D. M. Pickup, S. Ramos, X. Y. Lu, D. E. McNally, A. V. Chadwick, F. Giustino, T. Schmitt, L. C. Duda, M. R. Roberts, P. G. Bruce, *Nat. Chem.* **2018**, *10*, 288 – 295; d) B. M. de Boisse, S. Nishimura, E. Watanabe, L. Lander, A. Tsuchimoto, J. Kikkawa, E. Kobayashi, D. Asakura, M. Okubo, A. Yamada, *Adv. Energy Mater.* **2018**, *8*, 1800409; e) K. H. Dai, J. P. Wu, Z. Q. Zhuo, Q. H. Li, S. Sallis, J. Mao, G. Ai, C. H. Sun, Z. Y. Li, W. E. Gent, W. C. Chueh, Y. D. Chuang, R. Zeng, Z. X. Shen, F. Pan, S. S. Yan, L. F. J. Piper, Z. Hussain, G. Liu, W. L. Yang, *Joule* **2019**, *3*, 518 – 541.

[12] a) J. R. Croy, J. C. Garcia, H. Iddir, S. E. Trask, M. Balasubramanian, *J. Power Sources* **2020**, *471*, 228335; b) F. Dogan, B. R.

Long, J. R. Croy, K. G. Gallagher, H. Iddir, J. T. Russell, M. Balasubramanian, B. Key, *J. Am. Chem. Soc.* **2015**, *137*, 2328 – 2335.

[13] a) J. W. Somerville, R. A. House, N. Tapia-Ruiz, A. Sobkowiak, S. Ramos, A. V. Chadwick, M. R. Roberts, U. Maitra, P. G. Bruce, *J. Mater. Chem. A* **2018**, *6*, 5271 – 5275; b) C. F. Petersburg, Z. Li, N. A. Chernova, M. S. Whittingham, F. M. Alamgir, *J. Mater. Chem.* **2012**, *22*, 19993 – 20000.

[14] a) J. Xu, M. L. Sun, R. M. Qiao, S. E. Renfrew, L. Ma, T. P. Wu, S. Hwang, D. Nordlund, D. Su, K. Amine, J. Lu, B. D. McCloskey, W. L. Yang, W. Tong, *Nat. Commun.* **2018**, *9*, 947; b) W. Yang, T. P. Devereaux, *J. Power Sources* **2018**, *389*, 188 – 197; c) J. P. Wu, Q. H. Li, S. Sallis, Z. Q. Q. Zhuo, W. E. Gent, W. C. Chueh, S. S. Yan, Y. D. Chuang, W. L. Yang, *Condens. Matter* **2019**, *4*, 5.

[15] S. Roychoudhury, R. Qiao, Z. Zhuo, Q. Li, Y. Lyu, J. Kim, J. Liu, E. Lee, B. J. Polzin, J. Guo, S. Yan, Y. Hu, H. Li, D. Prendergast, W. Yang, *ChemRxiv* **2020**, https://doi.org/https://doi.org/10.26434/chemrxiv.11416374.v3.

[16] a) Z. Q. Zhuo, C. Das Pemmaraju, J. Vinson, C. J. Jia, B. Moritz, I. Lee, S. Sallies, Q. H. Li, J. P. Wu, K. H. Dai, Y. D. Chuang, Z. Hussain, F. Pan, T. P. Devereaux, W. L. Yang, *J. Phys. Chem. Lett.* **2018**, *9*, 6378 – 6384; b) Z. Q. Zhuo, Y. S. Liu, J. H. Guo, Y. D. Chuang, F. Pan, W. L. Yang, *J. Phys. Chem. Lett.* **2020**, *11*, 2618 – 2623.

[17] a) H. R. Chen, M. S. Islam, *Chem. Mater.* **2016**, *28*, 6656 – 6663; b) M. Ben Yahia, J. Vergnet, M. Saubanere, M. L. Doublet, *Nat. Mater.* **2019**, *18*, 496 – 502.

[18] Z. L. Chen, J. Li, X. C. Zeng, *J. Am. Chem. Soc.* **2019**, *141*, 10751 – 10759.

[19] A. Urban, I. Matts, A. Abdellahi, G. Ceder, *Adv. Energy Mater.* **2016**, *6*, 1600488.

[20] J. K. Nørskov, J. Rossmeisl, A. Logadottir, L. Lindqvist, J. R. Kitchin, T. Bligaard, H. Jónsson, *J. Phys. Chem. B* **2004**, *108*, 17886 – 17892.

[21] W. E. Gent, I. I. Abate, W. L. Yang, L. F. Nazar, W. C. Chueh, *Joule* **2020**, *4*, 1369 – 1397.

[22] a) Y. N. Zhang, S. Kim, G. Y. Feng, Y. Wang, L. Liu, G. Ceder, X. Li, *J. Electrochem. Soc.* **2018**, *165*, A1184 – A1192; b) X. Chen, S. Hwang, R. Chisnell, Y. C. Wang, F. Wu, S. Kim, J. W. Lynn, D. Su, X. Li, *Adv. Funct. Mater.* **2018**, *28*, 1803896; c) S. Kim, X. H. Ma, S. P. Ong, G. Ceder, *Phys. Chem. Chem. Phys.* **2012**, *14*, 15571 – 15578; d) Y. Takeda, K. Nakahara, M. Nishijima, N. Imanishi, O. Yamamoto, M. Takano, R. Kanno, *Mater. Res. Bull.* **1994**, *29*, 659 – 666.

[23] Y. J. Li, Y. R. Gao, X. F. Wang, X. Shen, Q. Y. Kong, R. C. Yu, G. Lu, Z. X. Wang, L. Q. Chen, *Nano Energy* **2018**, *47*, 519 – 526.

[24] X. Wang, G. Liu, T. Iwao, M. Okubo, A. Yamada, *J. Phys. Chem. C* **2014**, *118*, 2970.

Manuscript received: September 7, 2020
Revised manuscript received: November 16, 2020
Accepted manuscript online: December 15, 2020
Version of record online: March 30, 2021